Origin of high electrochemical stability of multi-metal chloride solid electrolytes for high energy all-solid-state lithium-ion batteries

Guofeng Xu [a,f], Liang Luo [b,d], Jianwen Liang [c], Shangqian Zhao [a,f], Rong Yang [a,f], Changhong Wang [c], Tianwei Yu [a,f], Limin Wang [e,f], Wei Xiao [e,f], Jiantao Wang [a,f,*], Jinqiu Yu [b,d,**], Xueliang Sun [c,***]

[a] *China Automotive Battery Research Institute Co., Ltd., Beijing 101407, China*
[b] *Rare Earth Functional Materials (Xiong'an) Innovation Center Co., Ltd., Xiong'an 071700, China*
[c] *Department of Mechanical and Materials Engineering, University of Western Ontario, London, Ontario, N6A 5B9 Canada*
[d] *National Engineering Research Center for Rare Earth Materials, GRINM Group Co., Ltd, Beijing 100088, China*
[e] *State Key Laboratory of Nonferrous Metals and Processes, GRINM Group Co., Ltd., Beijing 100088, China*
[f] *General Research Institute for Nonferrous Metals, Beijing 100088, China*

ARTICLE INFO

ABSTRACT

All-solid-state batteries (ASSBs) have gained substantial attention because of their intrinsic safety and potentially high energy density. To enable ASSBs, developing solid-state electrolytes (SSEs) with high electrochemical stability is of foremost significance. Here we report a multi-metal chloride SSEs with an excellent electrochemical stability (up to 4.5 V vs. Li^+/Li), which originates from the strong Zr-Cl bonding. In addition, a high room-temperature ionic conductivity of 1.58 mS/cm was achieved via increasing the Li vacancies in the structure as well as balancing carrier and vacancy concentration. Coupled with nickel-rich cathodes ($LiNi_{0.83}Co_{0.12}Mn_{0.05}O_2$) and high-voltage $LiCoO_2$ (4.5 V vs. Li^+/Li), ASSBs demonstrated superb electrochemical performance. This work provides an in-depth structural understanding of multi-metal chloride SSEs and feasible strategies to realize high-energy-density ASSBs.

1. Introduction

The next-generation all-solid-state batteries (ASSBs) using inorganic solid-state electrolytes (SSEs) have two outstanding advantages: guaranteed safety and the ability to easily achieving a high energy density of above 400 Wh/kg [1–4]. Researchers have made a lot of innovations and developed a series of inorganic ionic conductors including polymers, oxides, borohydrides and sulfides [5–14]. Among them, the high ionic conductivity of sulfides and the good chemical stability of oxides are particularly impressive [7,11,14]. However, the sulfide compounds have poor electrochemical stability and generate toxic H_2S gas in the humid air. The processing of oxide electrolyte-based electrode needs to exceed 1000 ℃, which negates its advantages. The electrochemical oxidation potential of the sulfide electrolyte is merely ~2.3 V vs. Li^+/Li, despite its high ionic conductivity, which makes the sulfide impossible to contact the cathode material directly. Researchers are committed to

developing SSEs with better performance in application prospects, halides with properties between sulfides and oxides seem to be a good choice of making the best use of their advantages and bypassing the disadvantages.

Since 2018, ternary chloride Li_3MCl_6 [15–20] and Zr doped Li_3MCl_6 (M = Y, In, Er, Sc, Yb, etc.) [21–25] have been intensively reported with ionic conductivity above 10^{-4} S/cm and electrochemical oxidation potential above 4 V vs. Li^+/Li, showing a promising prospect. The ionic transporting is dependent on the synthetic procedure, the local structural environment, and the site occupancy of M/ vacancy [18,19,21]. The ionic conductivity have been optimized via high throughput computation [26], Br^- anion doping [25,27,28], and structural adjustment [19,21,29]. The moisture tolerance was improved by adopting element In [16,17,30], the machinability could be enhanced by the using of Ga and F [31], and the interface between the electrolyte and both cathodes and Li-metal anode has been optimized as well [32–38].

However, the electrochemical oxidation potential of Li-M(III)-Cl materials has been calculated to be 4.2 V vs. Li$^+$/Li and tested to be ~4 V vs. Li$^+$/Li so far, which is inadequate to match with the commercial layered LiMO$_2$ (M = Ni, Co, Mn, and Al) cathodes of 4.3 V vs. Li$^+$/Li or above with high capacities.

Cyclic voltammetry (CV) measurement on a Li/SSE/Au blocking cell is generally adopted to evaluate the electrochemical stability window of the solid electrolytes. However, the results are inaccurate, considering carbon additives in electrode composites can trigger the decomposition of SSEs, especially at high working voltage, for the sufficient transporting of electrons matching the migration of Li$^+$ [39]. For instance, the electrochemical stability window of Li$_{10}$GeP$_2$S$_{12}$ [11] and Li$_6$PS$_5$Cl [40] was reported to 5 V tested by CV while it's not nearly that high practically. Mo [41] and Ceder [42] et al. used first-principles calculations to assess the electrochemical stability window of SSEs. The electrochemical window of sulfide SSEs was calculated as 1.7–2.4 V vs. Li/Li$^+$, which is much closer to the actual situation. The electrochemical stability window of Li$_3$YCl$_6$ and Li$_3$YBr$_6$ were calculated as 0.62–4.21 V and 0.59–3.15 V vs. Li/Li$^+$, which are much narrower than that measured using CV without carbon additives [43]. The oxidation potential of fluoride-based electrolytes can exceed 6 V vs. Li/Li$^+$, but the ionic conductivity has not been reported to exceed 1 mS/cm. The oxidation potential of bromide and iodide-based SSEs is only about 3 V vs. Li/Li$^+$. While the oxidation potential of chloride-based SSEs with high ionic conductivity is more than 4 V vs. Li/Li$^+$, and varies with the non-Li metal element, for the different thermodynamics of Cl$^-$ oxidation reactions. For instance, the thermodynamic electrochemical stability window of Li$_3$SmCl$_6$ and Li$_3$HoCl$_6$ are 0.67–4.23 V and 0.64–4.25 V vs. Li/Li$^+$.

Whereas few studies on the electrochemical stability of halide-based SSEs have been reported, and further experiments, calculations, and analyses are highly needed to improve the electrochemical stability and provide deep insights into the real electrochemical stability of the chloride SSEs.

Herein, we report a series of multi-metal chloride SSEs with a high-electrochemically stability (4.5 V vs. Li$^+$/Li), which are achieved by originally adopting non-Li metal elements with low cathodic limit as the non-Li metal element, and further introduction of stable Zr-Cl bond. All the CV tests herein use the electrode with carbon additives, the electrochemical window obtained by the test is very close to the theoretical value. The oxidation potential of the chloride electrolyte is high enough to be directly coupled with the bare cathode materials. A new revelation of local structure in the practical multi-metal chloride SSEs is discovered by perfectly combining first-principles calculation with an atomic-level observation of X-ray absorption spectroscopy. The electrochemical stable potential of Li-M-Cl materials depends largely on the characteristics of the non-Li metal element M. The fine structure of Li$_{2.556}$Yb$_{0.492}$Zr$_{0.492}$Cl$_6$ at different electrochemical states revealed using X-ray absorption spectroscopy confirmed the constant Zr-Cl bond of 2.3 Å and Zr centered spherical cluster. A general rule of ion transporting optimization scheme of Li-M-Cl electrolyte material has been explored via adopting a two-step method, which including the Li-deficiency and the synergistic effect of simultaneously regulating carrier concentration and vacancy concentration, through which the ion conductivity of Yb-based and Y-based chloride solid electrode are improved to both 1.58 mS/cm at room temperature (RT), and the all-solid-state cells using LiNi$_{0.83}$Co$_{0.12}$Mn$_{0.05}$O$_2$ (4.3 V vs. Li$^+$/Li) and LiCoO$_2$ (4.5 V vs. Li$^+$/Li) as cathode materials demonstrating excellent electrochemical performance.

2. Results and discussion

2.1. Design of electrochemically stable electrolyte

From the point of work function theory, the higher the ionization energy of the element, the lower the valence band maximum (VBM).

Element with lower electron energy of highest occupied molecular orbital (HOMO) is hard to lose electrons and has better oxidation stability, and element with higher electron energy of lowest unoccupied molecular orbital (LUMO) is hard to obtain electrons and has better reduction stability [43–46]. The relative electrochemical stability between compounds composed of various M elements can be evaluated by the band-gap width of HOMO-LUMO energy levels. In terms of atomic orbital theory, electron structures are stable when atomic orbitals are fully full, half full or empty according to the special cases of Hund's rule [47,48]. Li$_3$MCl$_6$ exhibits a stable octahedral structure for rapid transport of Li$^+$ when element M has a stable trivalent ion and the ion radius is around 80–90 pm. Among the seven elements that fit the criteria in Table 1, the valence electron structure of ytterbium is 4f^{14}6s^2, both the outermost 6s and 4f orbitals are in full state, while all the unused orbitals are in the empty state, all the orbital structures are stable, suggesting stable chemistry of Yb and a wider electrochemical window of Li-Yb-Cl.

The density of states (DOS) calculations was carried out to simulate the electrochemical stability by HOMO-LUMO band gap values, as shown in Figs. 1 and S1. Because the DOS diagram is aligned according to the deep energy level at ~45 eV, it is inappropriate of comparing oxidation and reduction stability simply by comparing the HOMO and LUMO energy values. Here, the oxidation and reduction potential of Li$_3$YbCl$_6$ and Li$_3$YCl$_6$ are simulated and intercompared by the cathodic limit and anodic limit after aligning the HOMO and LUMO values with their respective vacuum energy levels, as the dash area in Fig. 1 shows. The band-gap width of Li$_3$YCl$_6$ was calculated as 4.48 eV via the HOMO-LUMO method, which is narrower than the value based on Heyd-Scuseria-Ernzerhof functional [43], the value calculated using the same method can be compared with each other. The band-gap width of Li$_3$YbCl$_6$ with *Pnma* and *P-3m1* space group are 5.78 and 5.83 eV, both wider than that of the Li$_3$YCl$_6$, which implies the better electrochemical stability of Li$_3$YbCl$_6$ than Li$_3$YCl$_6$. The anodic limits of Li$_3$YbCl$_6$ with *Pnma* and *P-3m1* space group are 3.15 and 2.94 eV, higher than the 2.77 eV of the Li$_3$YCl$_6$, the cathodic limits are −2.63 and −2.89 eV, lower than −1.71 eV of the Li$_3$YCl$_6$, which indicates the higher oxidation potential and lower reduction potential of the Li$_3$YbCl$_6$. The anodic limit of Li$_3$YbCl with space group *Pnma* is higher than the *P-3m1* structure, which suggests the higher oxidation potential of the *Pnma* structural Li$_3$YbCl$_6$, and the favorable ability for the matching with layered cathode materials. The electrochemical stability of Li-M-Cl halide SSEs is not very relevant with the space group, but mainly depends on the characteristics of non-Li metal elements M. Density of states diagrams for other 5 Li$_3$MCl$_6$ materials in addition to Y and Yb are shown in Fig. S1, The HOMO-LUMO band gap identify with the trend of the electrochemical window calculated based on phase equilibrium [43,45]. It was expected that the oxidation potential of Li-M-Cl SSE is only related to the oxidation reaction of Cl$^-$, however, the calculation results here show that the oxidation potential of Cl$^-$ in different Li-M-Cl compounds is inconstant, which is related to the binding of M-Cl. Preliminary verification of the calculation is consistent with our previous design model, and it verified the feasibility of designing materials with high electrochemical stability by using work function theory and atomic orbital theory.

The crystal structure of the halide SSEs can be simply concluded into the following three categories: the monoclinic C2/m symmetric, including Li-In-Cl, Li-Sc-Cl, and most bromides; *Pnma* space group of the orthogonal crystal systems, involving the metastable Li-Y-Cl, Li-Yb-Cl, and Li-Lu-Cl. *P-3m1* space group structure of a trigonal system, including most Li-rare earth halide materials of Li-Re-Cl, as shown in Fig. 2a. The ionic conductivity of these three symmetric structures decreases successively, which is due to the increasing of the Li$^+$ migration energy barrier [49].

From the calculations and the preliminary verification results, our goal is determined to construct halide SSEs with high electrochemical stability via adopting element Yb into the Li-M-Cl material system. The energy above the hull of Li$_3$YbCl$_6$ with both *P-3m1* and *Pnma* space group is above 50 meV/atom as Table S1 shows, which are considered to

Table 1

Electron configuration and ionization energy for different elements with trivalent ionic radius of approximately 80–90 pm.

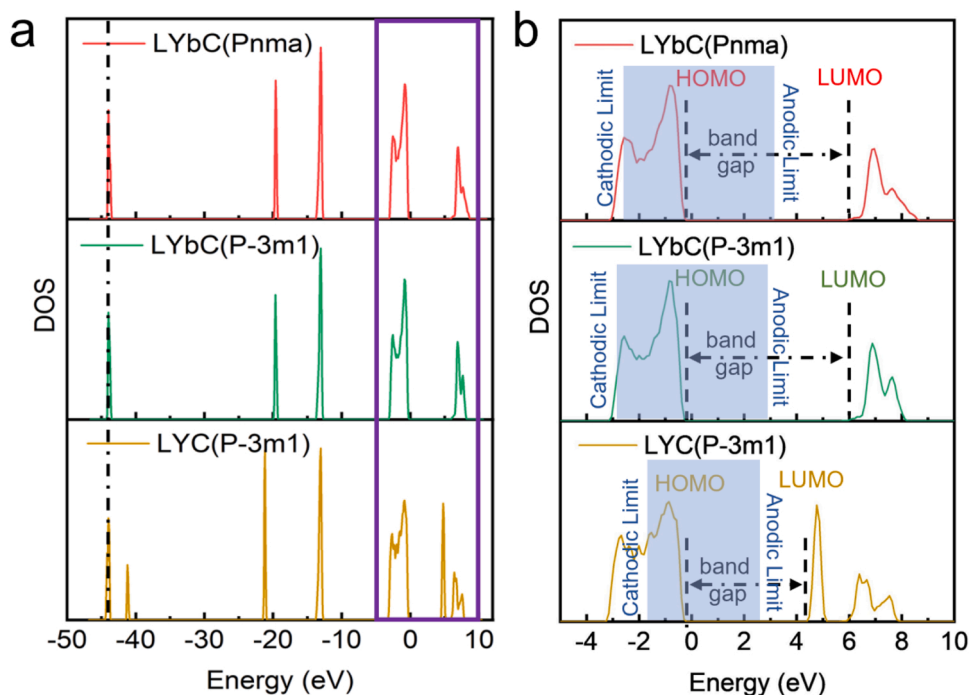|	Ho	Y	Er	Tm	Yb	Lu	In
Ionic radius /pm	90.1	90.0	89.0	88.0	86.8	86.1	80.0
Outer electron configuration	$4f^{11}6s^2$	$4d^15s^2$	$4f^{12}6s^2$	$4f^{13}6s^2$	**$4f^{14}6s^2$**	$5d^16s^2$	$5s^25p^1$
Ionization energy / kJ mol^{-1}	581.0	600.0	589.3	596.7	603.4	532.0	558.3

Fig. 1. The density of states diagrams of the Li_3YbCl_6 with *Pnma* and *P-3m1* space group and Li_3YCl_6. (a) Diagrams aligned according to the deep energy level at ~45 eV. (b) Partial enlargement of (a) over the energy range of −5 to 10 eV.

be unstable and unsynthesizable. However, as Fig. 2b shows, the controllable preparations of Li_3YbCl_6 electrolyte materials with both space groups of *P-3m1* and *Pnma* are achieved by simply adjusting the preparation process conditions of a high-temperature melting method. This suggests that the conditions used to judge whether the material can exist stably through energy above hull are with certain limitations and easy to mislead the experiment and it is important to verify the calculated results through actual experiments. Meanwhile, Li_3YbCl_6 shows good electrochemical oxidation stability. The forward and reverse linear voltammetry curves in Fig. 2c of the *Pnma* symmetrical Li_3YbCl_6 indicate that it could maintain electrochemical stability at 4.5 V vs. Li^+/Li. In Fig. 2d, the electrochemical stability of Li_3YbCl_6, Li_3YCl_6, and Li_3InCl_6 are compared with cyclic voltammetry curves, it was found that the stability of Li_3YbCl_6 is much better than the others in terms of both initial reaction potential and electrochemical reaction degree. The impedance of Li_3YbCl_6 for the *Pnma* space group is lower than that of the *P-3m1* space group as the electrochemical impedance spectroscopy (EIS) of Fig. 2e shows. The diffusion energy barrier of lithium-ion calculated by first-principles in Fig. S2 also displays that the theoretical conductivity of Li_3YbCl_6 for the *Pnma* space group is much higher than that of the *P-3m1* space group.

2.2. Optimization of Li^+ migration property

Herein, a general two-step method is proposed to improve the ionic conductivity of halide SSEs, the first step is the Li-deficiency strategy, the second is the synergistic effect of carrier concentration and vacancy concentration. Firstly, samples of $Li_{3-x}Yb_{1+x}Cl_6$ (x = 0.017, 0.034, 0.053, 0.071) with different levels of lithium-deficiency were

synthesized to initiatively create lithium vacancies. The Yb^{3+} has a charge of plus three and Li^+ has a charge of plus one, when one Yb^{3+} ion replaces one Li^+ ion, two Li vacancies are created in order to maintain charge balance [20,21]. As shown in Fig. 3a–c, all the prepared samples present crystal structure with the *Pnma* space group of the orthogonal crystal system. The X-ray diffraction peaks slightly shift to the left with the increase of Yb substitution, as show in Fig. 3b and c. According to the Bragg's equation, the left shift of the XRD peak represents a decrease of the spacing between the crystal planes. Considering that when one Yb atom enters the lattice, three Li atoms must come out to create Li vacancies, therefore, the left shift of the XRD peaks indicates the successful Yb doping on Li-site. The decrease of the impedance is attributed to the decrease of the energy barrier caused by the introduction of lithium vacancies. However, with the continuous introduction of Li vacancies, the increase of $YbCl_3$ impurity leads to the decrease of ionic conductance instead. As Fig. S3 shows, the XRD pattern of sample $Li_{3-3x}Yb_{1+x}Cl_6$ (x = 0.053) following Rietveld refinement was performed, and the refinement converged to the final stoichiometry of $Li_{2.852}Yb_{1.049}Cl_6$, which means the successful creating of lithium vacancies. In addition, the refined results show that the cell parameters increase with the doping of Yb, as shown in Table S2. When the Yb-doping amount is x = 0, the cell volume is 861.193 Å^3 and when doping amount increases to x = 0.034, the cell volume increases to 862.349 Å^3. The increased cell parameter provides better kinetic condition for the migrating through the lattice of Li^+, as a result, the ionic conductivity increases from 0.2 mS/cm to 0.5 mS/cm with the Yb-doping amount increasing from x = 0 to x = 0.034. When the Yb-doping amount continues to increase to x = 0.053, the cell volume increases to 863.018 Å^3, however, the decrease of Li^+ carrier concentration begins to affect the ionic
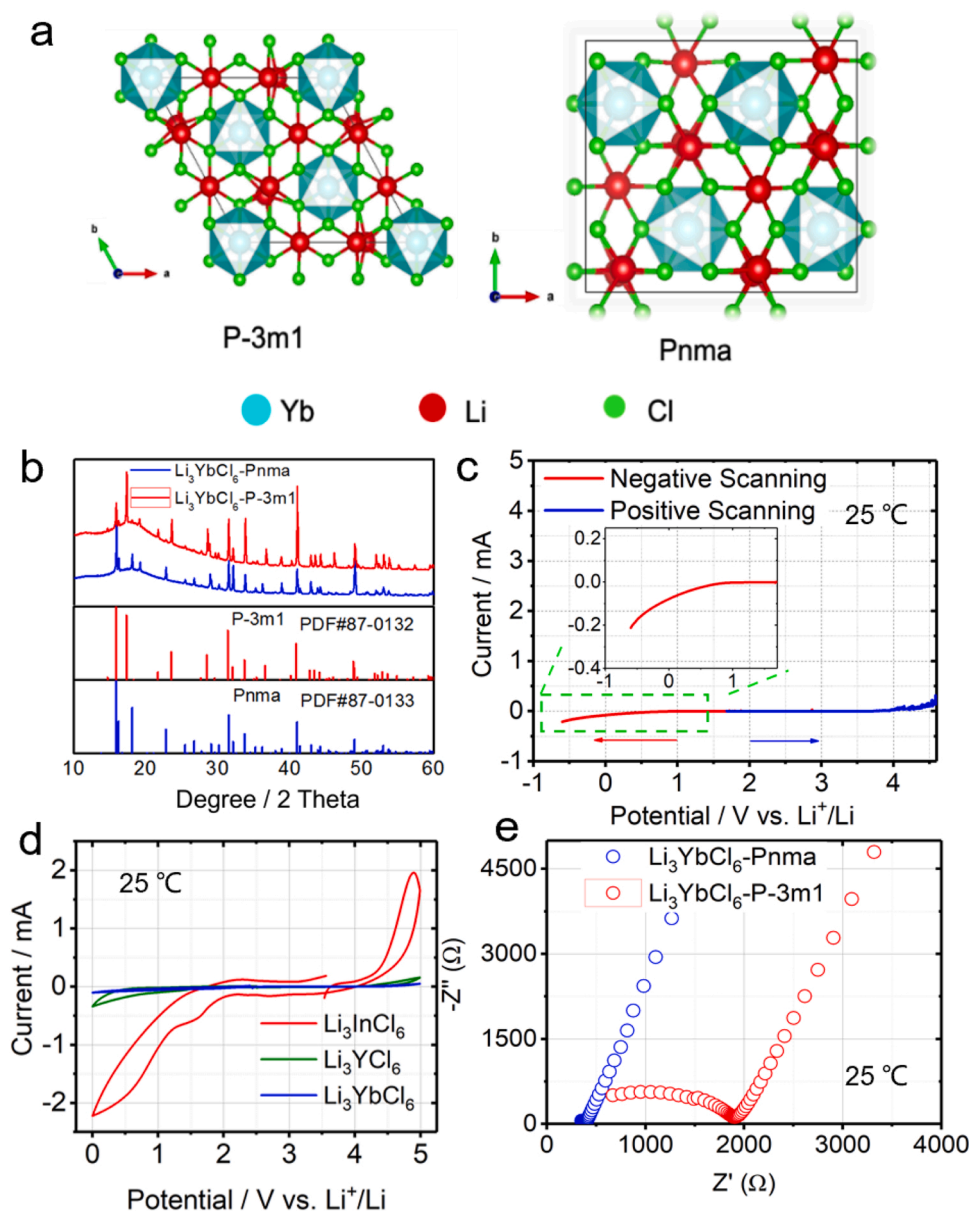
Fig. 2. (a) Ionic arrangement of trigonal and orthorhombic structure of Li_3YbCl_6. (b) X-ray diffraction patterns of Li_3YbCl_6 with *Pnma* and *P-3m1* space group. (c) Negative (ocv~−0.6 V) and positive (ocv~4.6 V) linear voltammetry scanning curves. (d) Cyclic voltammetry curves, (e) Nyquist plots of Li_3YbCl_6 with *Pnma* and *P-3m1* space group for Li^+-blocking symmetric BE/C/SSE/C/BE cells at RT.

conductivity, resulting in the ionic conductivity of $Li_{3-3x}Yb_{1+x}Cl_6$ (x = 0.053) decreased to 0.4 mS/cm. Therefore, the approach of creating lithium vacancies through Yb-doping has limited effect on the improvement of ionic conductivity, and more efficient strategies should be developed to co-regulate the lithium vacancies and the concentration of Li^+ carrier. Ab initio molecular dynamics (AIMD) of first-principles calculation is adopted in order to explore the effect of lithium-deficiency on lithium migration. The materials with the occupancy rate of x = 0.0417, 0.0625 and 0.083 in $Li_{3-3x}Yb_{1+x}Cl_6$ were calculated and the theoretical ionic conductance at RT is 11.024 mS/cm when x = 0.083, twice of the initial Li_3YbCl_6, which is in accordance with the experimental results of 2.5 times, as shown in Fig. S4. The difference between the measured and calculated values of the ionic conductivity is revealed as channel-blocking defects of the susceptible 1D diffusion channel [43].

The second step not only considered the increasing of Li vacancies through multivalent cation doping but also took into account the adjustment of Li^+ carrier concentration to achieve the synergistic effect

of vacancies and carrier concentration, which compensates for the loss of lithium ions after the addition of multivalent cations. On the optimal condition that Zr^{4+} replaced 50% of M^{3+} according to Nazar's research [21], the content of Li was further adjusted to increase the concentration of lithium carrier based on the basic component $Li_{2.5}Yb_{0.5}Zr_{0.5}Cl_6$. As shown in Fig. 3d, all the samples prepared to demonstrate crystalline with the *Pnma* space group of the orthogonal crystal system after Zr doping. The X-ray diffraction peaks between 30° and 38° of $Li_{2.556}Yb_{0.492}Zr_{0.492}Cl_6$ (y = 0.016) sample slightly shifts to the right in Fig. 3e and f, which indicates a smaller crystalline interplanar spacing. It is assumed that the synergistic effect of Li vacancy concentration and Li^+ carrier concentration achieves the effect of the lowest ion migration barrier, which enhances the ionic conductivity of Yb-based chloride solid electrolyte to 1.58 mS/cm at RT by sample $Li_{2.556}Yb_{0.492}Zr_{0.492}Cl_6$, as demonstrated in Fig. 3h. Superimposed electrochemical processes of the electrodes have been analyzed by the relaxation time distribution (DRT) method in Fig. S5, the spectra were calculated from the impedance plots of Fig. 3g to separate the bulk and grain boundary resistances.
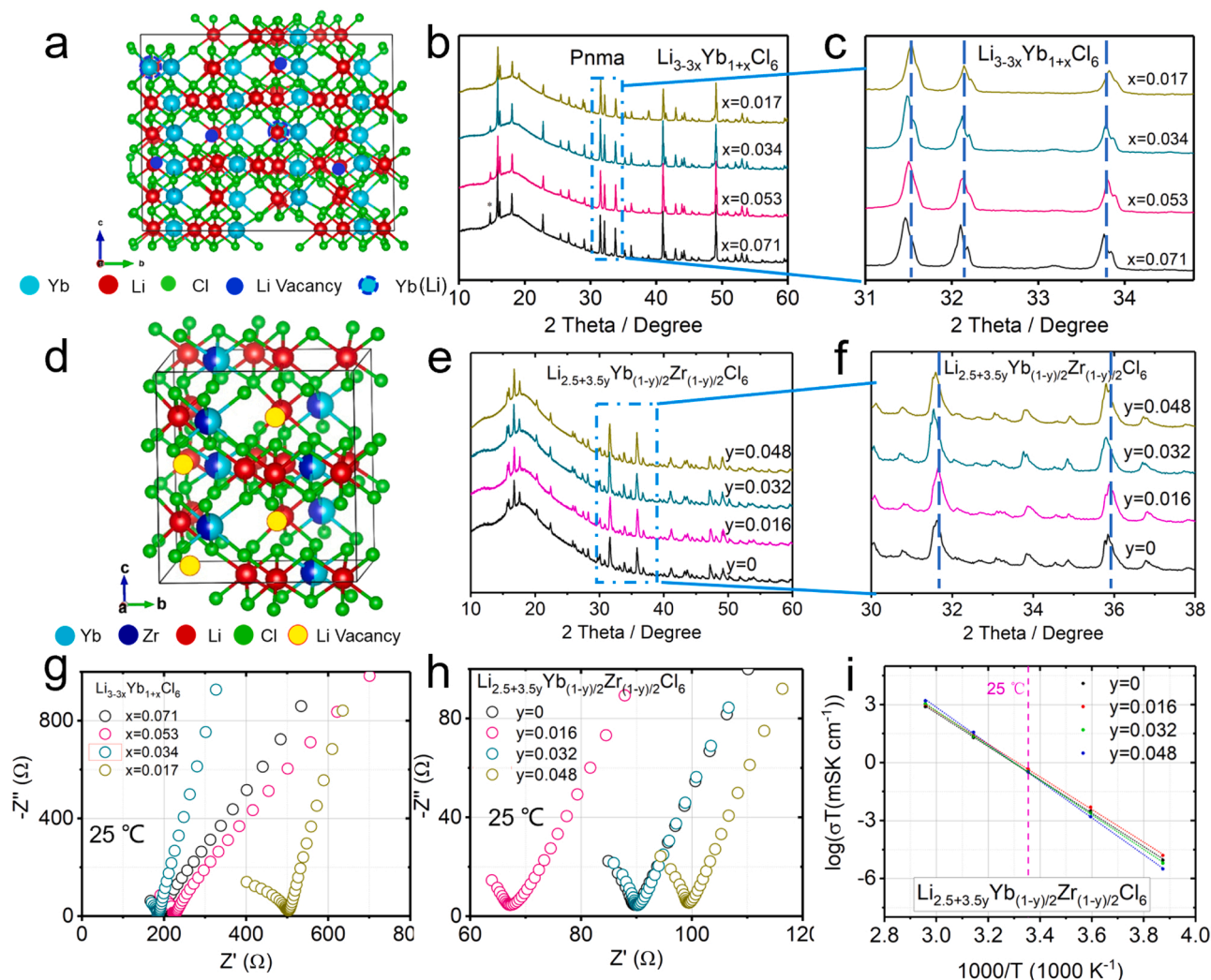
Fig. 3. (a–c) Ionic arrangement and XRD diffraction patterns for $Li_{3-3x}Yb_{1+x}Cl_6$ (x = 0.017, 0.034, 0.053, 0.071). (d–f) ionic arrangement and XRD diffraction patterns for $Li_{2.5+3.5y}Yb_{(1-y)/2}Zr_{(1-y)/2}Cl_6$ (y = 0, 0.016, 0.032, 0.048), (g, h) Nyquist plots at RT, (i) Arrhenius plots of $Li_{2.5+3.5y}Yb_{(1-y)/2}Zr_{(1-y)/2}Cl_6$ (y = 0, 0.016, 0.032, 0.048).

The major peak components at the higher and lower frequency were attributed to resistance in the bulk and grain boundary, respectively, for the ionic transport in the pellets of single-phase material [50]. The ratio of bulk impedance to grain boundary impedance is 1:4, so the apparent ionic conductivity is 20% of bulk ionic conductivity. For the sample of 1.58 mS/cm, the bulk ionic conductivity should be 7.9 mS/cm, which is closer to the result calculated by the AIMD method in Fig. S5. Fig. 3i shows the Arrhenius curves, the corresponding activation energies (E_a) calculated based on Arrhenius equation are 0.324, 0.317, 0.336, 0.358 eV, which are comparable to reported halide SSEs. In addition, the electronic conductivity of the $Li_{2.556}Yb_{0.492}Zr_{0.492}Cl_6$ sample was tested to $3.7*10^{-9}$ S/cm as Fig. S6 shows. The strategy also works for Y-based chloride $Li_{2.766}Y_{0.462}Zr_{0.462}Cl_6$, as is shown in Fig. S7. As thus, a universal two-step method is proposed to improve the ionic conductivity of chloride solid electrolytes. The substitution of different amounts of Zr^{4+} results in different activation energy, as is simulated in Fig. S8.

Fig. 4a shows the X-ray diffraction (XRD) patterns of the $Li_{2.556}Yb_{0.492}Zr_{0.492}Cl_6$ sample and its fitting resulting from the Rietveld refinement. The crystal structure can be indexed to Phase-III with the *Pnma* space group of the orthorhombic crystal system [21]. The lattice parameters converged to a = 12.78 Å, b = 11.05 Å, c = 6.00 Å, $\alpha = \beta = \gamma = 90°$. The crystal structure displays the same occupancy of Zr and Yb, with a slightly smaller value in y-coordinate than the

Pnma-phase Li_3YbCl_6, due to the smaller ionic radius of Zr^{4+}. The optimal ionic conductivities of the Li-Er-Zr-Cl and Li-Y-Zr-Cl series of SSEs obtained in Nazar's group were 1.1 and 1.4 mS/cm, respectively, when the substitution amounts of Zr to M is 50%. The excellent ion transport property is obtained due to the introduction of a new Li3 site by Zr doping [21]. Herein, the concentration of the carrier Li^+ is slightly increased, to further improve the ion conductivities of the Li-Yb-Zr-Cl and Li-Y-Zr-Cl series of SSEs to both 1.58 mS/cm, which is due to the synergistic effect of Li^+ carrier and Li vacancy concentration.

Zirconium K-edge X-ray absorption fine structure (XAFS) was employed to reveal the local environment around the Zr atoms of the $Li_{2.556}Yb_{0.492}Zr_{0.492}Cl_6$ SSE before and after electrochemical cycling. Fig. 4b and c show the normalized K-edge XAFS spectra and the corresponding $\chi(k)$ spectra [51] of $Li_{2.556}Yb_{0.492}Zr_{0.492}Cl_6$ before and after 30 cycles with $LiNi_{0.83}Co_{0.12}Mn_{0.05}O_2$. The identical main edge position at ~18020 eV indicates the constant tetravalent oxidation state of Zr [23, 52]. Three differences are observed in the zone I, II, and III, especially in the zone I, which is related to the Zr2/Zr3 site disorder [21]. The sharpened peak in the region I is due to the reconstruction of the Zr2/Zr3 disorder during the electrochemical process. Fig. 4d shows the R space $\chi(R)$ spectra of pristine $Li_{2.556}Yb_{0.492}Zr_{0.492}Cl_6$, the strongest peak at a distance of ~2.3 Å expresses the shortest Zr-Cl coordination of octahedral $ZrCl_6^{2-}$ and the multiple peaks display the long-range ordering of
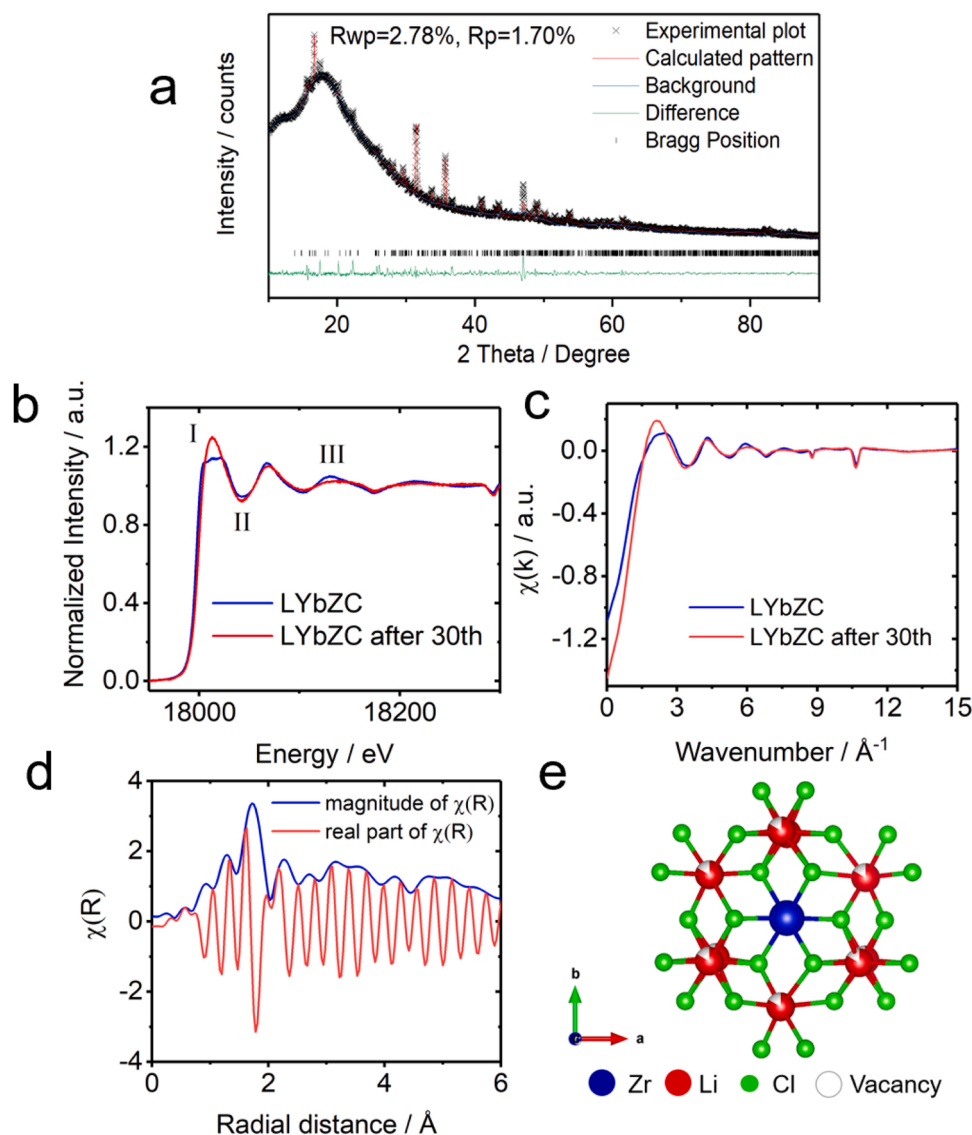
Fig. 4. (a) Observed and calculated powder X-ray Rietveld refinement profiles for $Li_{2.556}Yb_{0.492}Zr_{0.492}Cl_6$. (b) Normalized Zr K-edge XAFS spectra, (c) the corresponding $\chi(k)$ spectra of $Li_{2.556}Yb_{0.492}Zr_{0.492}Cl_6$ before and after 30 cycles with $LiNi_{0.83}Co_{0.12}Mn_{0.05}O_2$. (d) Corresponding $\chi(R)$ spectra, (e) Zr centered spherical cluster of $Li_{2.556}Yb_{0.492}Zr_{0.492}Cl_6$.

the Zr centered coordination. Fig. 4e demonstrates the local structure coordination of the two shells adjacent to the central Zr atom, the 1st shell illustrates the Zr-Cl bond of the regular octahedral $ZrCl_6^{2-}$, and the 2nd shell presents Li-Cl bond, with different possible occupancies of Li atom and vacancy, as is shown in Fig. S9.

2.3. Electrochemical performance and mechanism

As can be seen from Fig. 5a, the electrochemical reaction degree of the optimized $Li_{2.556}Yb_{0.492}Zr_{0.492}Cl_6$ sample is much less than that of the initial sample Li_3YbCl_6 and Li_3YCl_6, considering that the electrochemical reaction degree can be expressed by integral area, which means the electrochemical stability is further improved via the introduction of zirconium. The cyclic voltammetry curve shows good reversibility after 20 cycles in Fig. 5b. For the oxidation process, the current density is 10^{-5} mA/mg at the cut-off voltage of 4.5 V vs. Li^+/Li, and remains stable as the cycle goes on. While for the reduction process, the current density at the cut-off voltage of 0 V increases gradually as the cycle progresses, and reaches 10^{-4} mA/mg after 20 cycles, indicating that the chloride electrolytes can be directly contacted with the high-

voltage layered cathodes, but cannot be coupled with the lithium anode to construct the battery. Therefore, Li-In alloy anode is necessary. Besides, calculated mechanical properties in Table S3 suggest the Yb-based chloride exhibits better mechanical flexibility than Y- and In-based chloride, and the chemical stability of the material in air is also improved by the introduction of Zr, as shown in Fig. S10, the $Li_{2.556}Yb_{0.492}Zr_{0.492}Cl_6$ sample delivers ionic conductivity of 1.1 mS/cm after exposing to an environment with dew point temperature of −40 °C for 24 h, the ionic conductivity retention of the $Li_{2.556}Yb_{0.492}Zr_{0.492}Cl_6$ sample is 76.4%, while the retention of Li_3YbCl_6 is only 26.6%. Based on the theoretical calculations by Mo et al. [12], the improvement of moisture stability for chloride solid electrolytes is due to the adjusting of hydrolysis reaction energy by doping/substituting proper cations.

The outstanding electrochemical and chemical stability suggest the excellent application prospect of the Yb-based chloride electrolyte for ASSBs with high energy density. The electrochemical properties of the $Li_{2.556}Yb_{0.492}Zr_{0.492}Cl_6$ sample matched with high voltage cathode materials were investigated. Because the potential of Li^+ intercalation for Li-In alloy is 0.6 V higher than that of the lithium anode, so the cut-off voltage of 3.7 V and 3.9 V vs. Li^+/Li-In in Fig. 5c and e are exactly
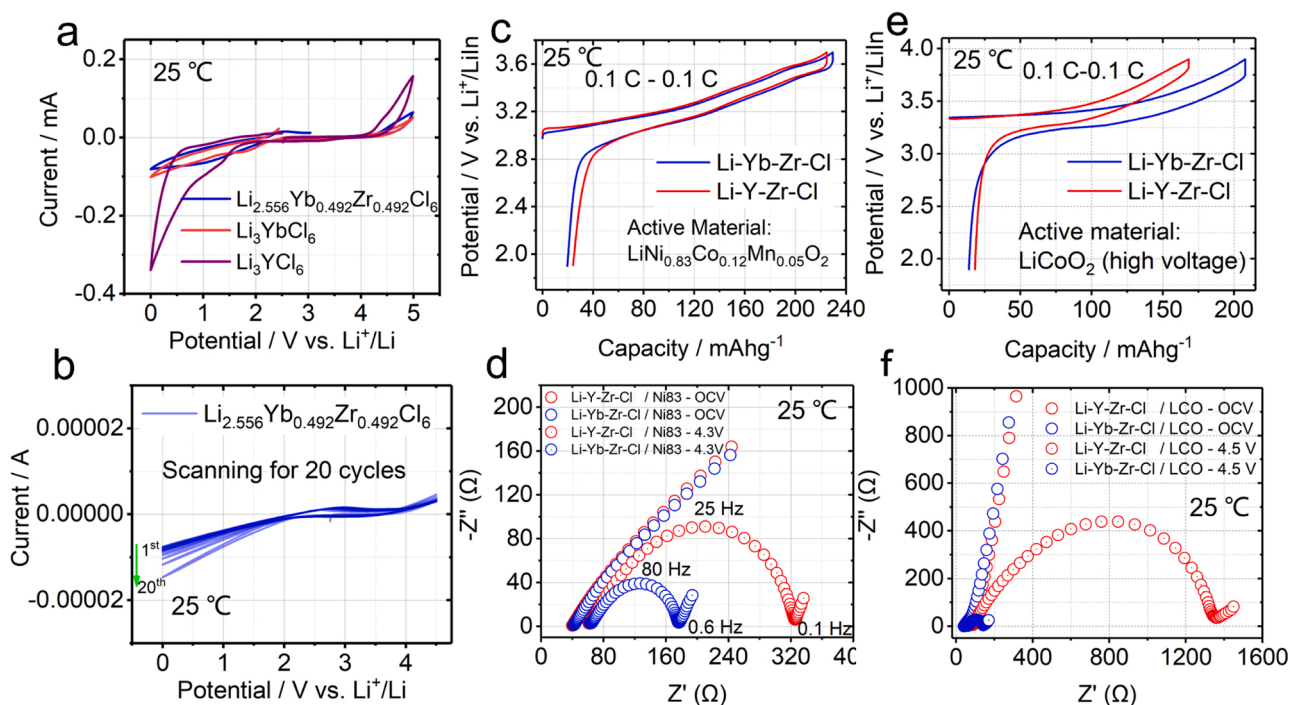
Fig. 5. (a,b) Cyclic voltammetry curves, (c) The initial charge-discharge curves and (d) electrochemical impedance spectroscopy for $LiNi_{0.83}Co_{0.12}Mn_{0.05}O_2$, (e) initial charge-discharge curves and (f) electrochemical impedance spectroscopy for high voltage $LiCoO_2$ with SSEs of $Li_{2.556}Yb_{0.492}Zr_{0.492}Cl_6$ and $Li_{2.766}Y_{0.462}Zr_{0.462}Cl_6$.

4.3 V vs. Li^+/Li and 4.5 V vs. Li^+/Li, respectively. As shown in Fig. 5c, single-crystalline $LiNi_{0.83}Co_{0.12}Mn_{0.05}O_2$ (simplified as NCM83) exhibits discharge specific capacity of 209.8 mAh/g and coulombic efficiency of 91.5% at a charge-discharge rate of 0.1 C (20 mA/g), while the Li-Y-Zr-Cl electrolyte delivers a lower specific capacity of 200.6 mAh/g and coulombic efficiency of 89.3%. The Li-Yb-Zr-Cl

$(Li_{2.556}Yb_{0.492}Zr_{0.492}Cl_6)$/NCM83 electrode shows a smaller loss of reversible capacity than the Li-Y-Zr-Cl($Li_{2.766}Y_{0.462}Zr_{0.462}Cl_6$)/NCM83 electrode. The sulfide with good reduction stability is needed as a buffer layer to isolate the chloride and the anode [49]. The phenomenon was further explored through electrochemical impedance spectroscopy as is shown in Fig. 5d. The charge transfer impedance in the intermediate
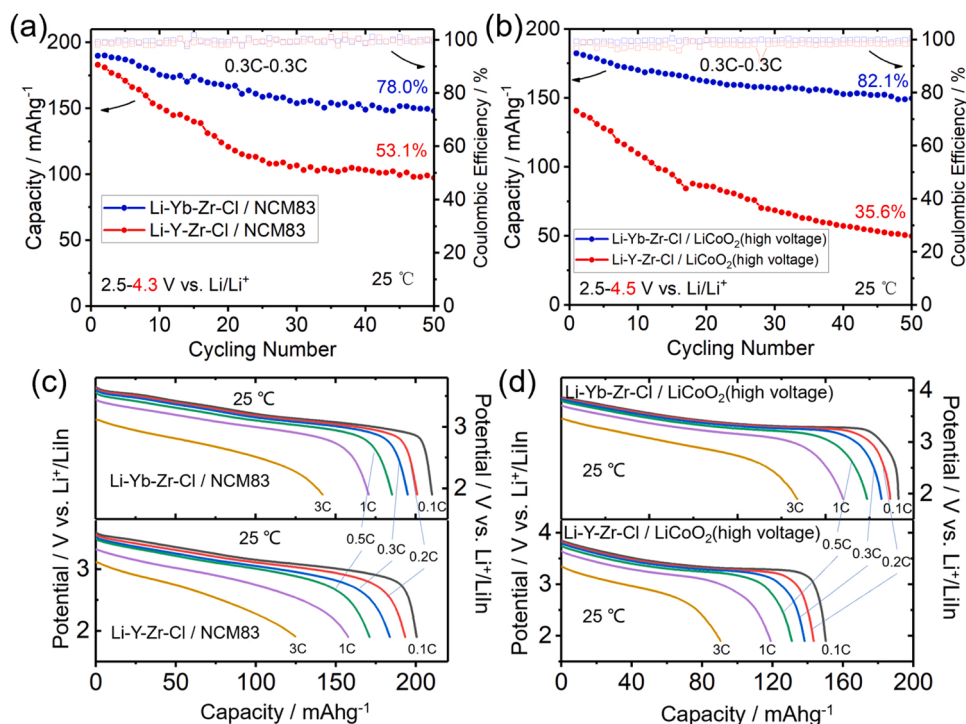

Fig. 6. (a, b) Cycle performance at 0.3 C (60 mA/g) and (c, d) rate capability for $LiNi_{0.83}Co_{0.12}Mn_{0.05}O_2$ and high voltage $LiCoO_2$ with SSEs of $Li_{2.556}Yb_{0.492}Zr_{0.492}Cl_6$ and $Li_{2.766}Y_{0.462}Zr_{0.462}Cl_6$.

frequency region of the Li-Yb-Zr-Cl/NCM83 electrode is significantly lower than that of the Li-Y-Zr-Cl/NCM83 electrode when the electrode is charged to 4.3 V vs Li/Li$^+$, which indicates that the interface impedance of the Yb-based electrode is much smaller at high potential region. Combined with the cyclic voltammetry curves of the SSEs, it can be seen that the electrochemical decomposition reaction of the Y-based electrolyte occurs below 4.3 V vs Li/Li$^+$.

The Yb-based chloride SSE is electrochemically stable at 4.5 V, it is expected to match the cathode material with high voltage to construct the ASSBs with high energy density. Here, LiCoO$_2$ with a stable electrochemical property at 4.5 V vs. Li/Li$^+$ was used to verify the electrochemical stability of different electrolytes. The charge-discharge curves in Fig. 5e show that LiCoO$_2$ exhibits discharge specific capacity of 193.9 mAh/g and coulombic efficiency of 93.3% at a charging cut-off voltage of 4.5 V vs Li/Li$^+$, while the Li-Y-Zr-Cl electrolyte delivers a lower specific capacity of 150.0 mAh/g and coulombic efficiency of 89.2%. Electrochemical impedance spectroscopy was measured at different electrochemical states, as is shown in Fig. 5f. The impedance of Yb and Y electrodes is similar at open-circuit voltage (OCV), however, charge transfer impedance in the intermediate frequency region of the Li-Yb-Zr-Cl/LCO electrode is dramatically lower than that of the Li-Y-Zr-Cl/LCO electrode when the electrode is charged to 4.5 V vs Li/Li$^+$, indicating the very low electrochemical sensitivity of Yb-based chloride electrode.

As shown in Fig. 6a and b, after the 50th electrochemical cycle at 0.3 C at the voltage range of 2.5–4.3 V versus Li$^+$/Li, the Li-Yb-Zr-Cl/NCM83 electrode delivers the discharge capacity of 148.1 mAh/g, which is about 78.0% of its initial discharge capacity. As comparison, the discharge capacity of Li-Y-Zr-Cl/NCM83 electrode after 50 cycles can only achieve 97.3 mAh/g (53.1% of capacity retention). After the 50th electrochemical cycle at 0.3 C at the voltage range of 2.5–4.5 V versus Li$^+$/Li, the Li-Yb-Zr-Cl/ LiCoO$_2$ electrode delivers the discharge capacity of 149.7 mAh/g, which is about 82.1% of its initial discharge capacity. While the discharge capacity of Li-Y-Zr-Cl/ LiCoO$_2$ electrode after 50 cycles can only achieve 49.9 mAh/g (35.6% of capacity retention). Moreover, the coulomb efficiency of the Li-Yb-Zr-Cl/LiCoO$_2$ electrode is higher than that of the Li-Y-Zr-Cl/ LiCoO$_2$ electrode. As for the rate capability, the Li-Yb-Zr-Cl/NCM83 electrode delivers the discharge capacities of 170.6 mAh/g and 141.8 mAh/g at 1 C and 3 C,

respectively. Whereas the Li-Y-Zr-Cl/NCM83 electrode delivers that of 157.7 mAh/g and 124.6 mAh/g. The Li-Yb-Zr-Cl/LiCoO$_2$ electrode shows the discharge capacities of 160.0 mAh/g and 134.0 mAh/g at 1 C and 3 C, respectively, much higher than 119.0 mAh/g and 90.4 mAh/g of the Li-Y-Zr-Cl/LiCoO$_2$ electrode at the voltage range of 2.5–4.5 V versus Li$^+$/Li, as Fig. 6c and d shows. It can be indicated that the higher the voltage, the more obvious the electrochemical advantage of Li-Yb-Zr-Cl for Li-Y-Zr-Cl solid electrolyte.

X-ray photoelectron spectroscopy (XPS) measurements of Li$_{2.556}$Yb$_{0.492}$Zr$_{0.492}$Cl$_6$ and Li$_{2.766}$Y$_{0.462}$Zr$_{0.462}$Cl$_6$ before and after electrochemical cycling with LiNi$_{0.83}$Co$_{0.12}$Mn$_{0.05}$O$_2$ were carried out to reveal the surface chemistry changes during the electrochemical process, as are shown in Fig. 7a and b. After the 30th of electrochemical cycling, the Y3d spectrum of Li$_{2.766}$Y$_{0.462}$Zr$_{0.462}$Cl$_6$(LYZC)/NCM83 electrode displays oxygen-containing substances which can be indexed to Y$_2$O$_3$/Y$_2$(CO$_3$)$_3$ according to Janek's research [35]. While the Yb4d spectrum of Li$_{2.556}$Yb$_{0.492}$Zr$_{0.492}$Cl$_6$(LYbZC)/NCM83 electrode remains the same as the pristine Li$_{2.556}$Yb$_{0.492}$Zr$_{0.492}$Cl$_6$.

Ex-situ Zirconium K-edge X-ray absorption fine structure was also employed to observe the local structure of the Li$_{2.556}$Yb$_{0.492}$Zr$_{0.492}$Cl$_6$ at different electrochemical states. The overall normalized Zr K-edge spectra are shown in Fig. 8a, the corresponding $k^2\chi(k)$, $\chi(R)$, $\chi(q)$ spectra of k space, R space, and q space are presented in Fig. 8(b–d). The whole spectrum, including the details of peak position, did not show significant changes, which indicates the local structural environment of the Zr atom is stable under different electrochemical states, even after 30th electrochemical cycles with LiNi$_{0.83}$Co$_{0.12}$Mn$_{0.05}$O$_2$. The constant Zr-Cl bond of ~2.3 Å is obviously smaller than the Zr-Cl bond of Li$_2$ZrCl$_6$ [23]. Which explains the elevated ionic conductivity and enhanced electrochemical stability observed in CV curves with the doping of Zr into the Li-M-Cl system. The trough at 10 Å^{-1} of wavenumber in k space for $k^2\chi(k)$ and q space can be indexed to the lithium vacancies at the second shell of the Zr centered spherical cluster, indicates the Zr helps remain the stability of the crystal structure under the circumstance of introducing extra lithium vacancies.
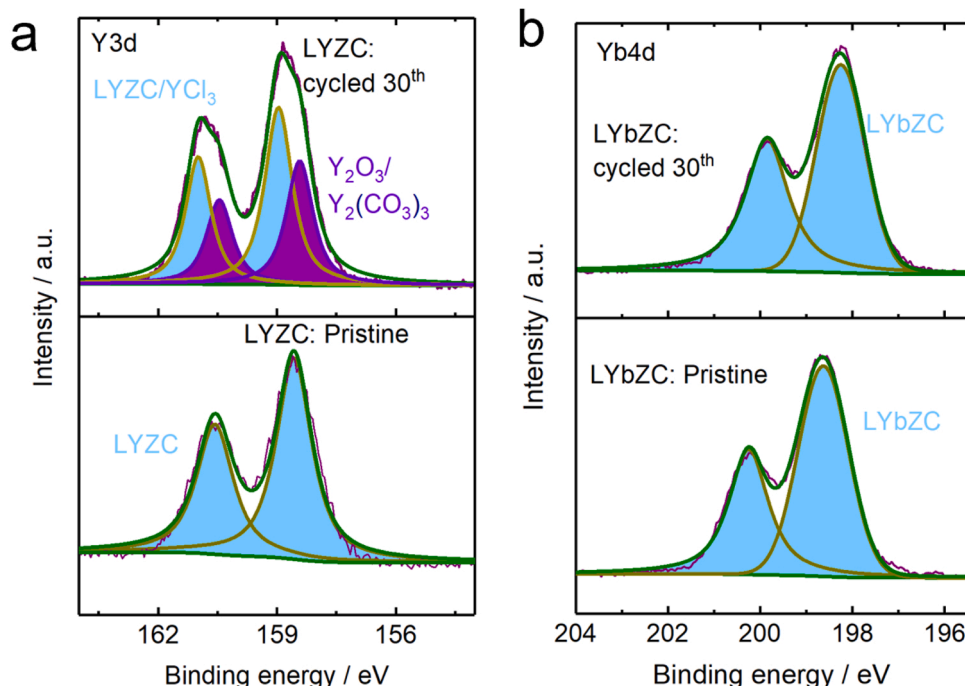

Fig. 7. X-ray photoelectron spectroscopy of (a) Li$_{2.766}$Y$_{0.462}$Zr$_{0.462}$Cl$_6$ and (b) Li$_{2.556}$Yb$_{0.492}$Zr$_{0.492}$Cl$_6$ before and after 30 cycles with LiNi$_{0.83}$Co$_{0.12}$Mn$_{0.05}$O$_2$.
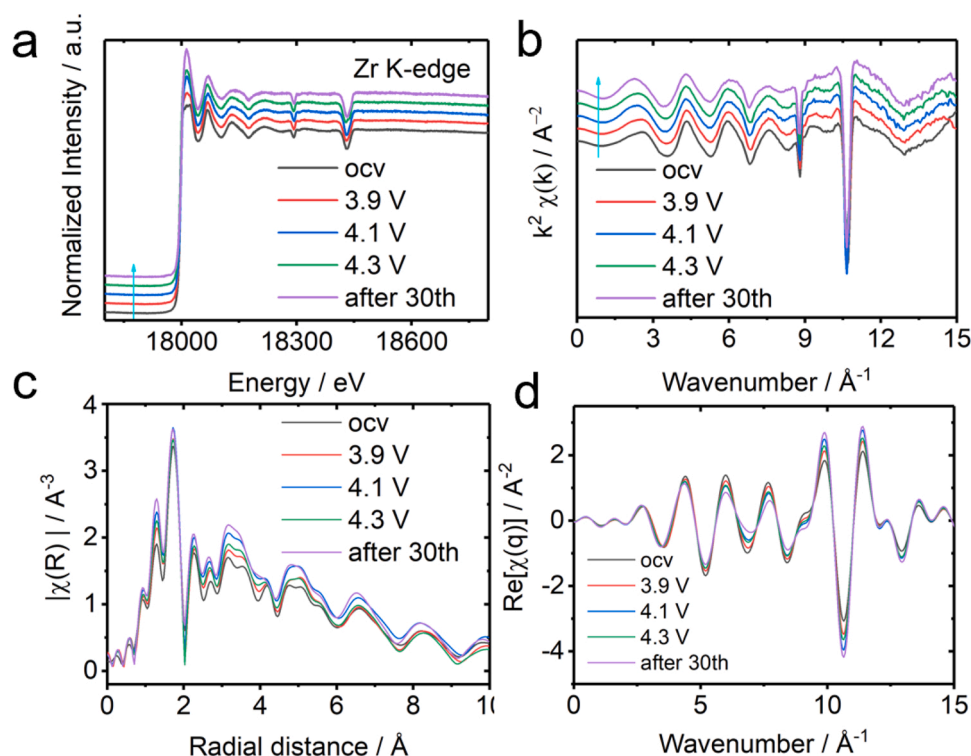
Fig. 8. *Ex-situ* Zr K-edge XAFS (a) normalized spectra, (b) $k^2\chi(k)$, (c) $\chi(R)$, (d) $\chi(q)$ spectra of $Li_{2.556}Yb_{0.492}Zr_{0.492}Cl_6$/NCM83 cathode composites at different electrochemical states.

3. Conclusion

In summary, chloride solid electrolyte with excellent electrochemical stability is designed ab initio based on work function and atomic orbital theories, ytterbium is perceived as the optimal non-Li metal element of Li-M-Cl SSEs for the low cathodic limit and fully full atomic orbitals. The electrochemical stable potential of Li-M-Cl materials depends largely on the characteristics of the non-Li metal element M and Li-Yb-Cl shows excellent electrochemical oxidation stability above 4.5 V vs. (Li^+/Li). A general two-step method to improve the ionic conductivity of halide SSEs by Li-deficiency strategy and the synergistic effect of carrier concentration and vacancy concentration is proposed, the ion conductivities of Yb-based and Y-based chloride SSEs are elevated to both 1.58 mS/cm. The fine structures of $Li_{2.556}Yb_{0.492}Zr_{0.492}Cl_6$ at different electrochemical states are revealed, constant Zr-Cl bond of 2.3 Å and Zr centered spherical cluster has been confirmed. The electrochemical stability above 4.5 V vs. Li^+/Li is insured by originally adopting ytterbium as the non-Li metal element, and further enhanced by the introduction of stable Zr-Cl bond, which makes the all-solid-state cells using $LiNi_{0.83}Co_{0.12}Mn_{0.05}O_2$ (4.3 V vs. Li^+/Li) and $LiCoO_2$ (4.5 V vs. Li^+/Li) as cathode materials demonstrating excellent electrochemical performance. It offers a good prospect of constructing ASSBs with high energy density by using high-voltage cathode materials such as Li-rich manganese-based material of 4.6–4.8 V vs. Li^+/Li and spinel $LiNi_{0.5}Mn_{1.5}O_4$ of 4.8–5.0 V vs. Li^+/Li. And the results further provide new guidance to the designing and exploiting for SSEs with wide electrochemical windows, high ion transporting efficiency and excellent application properties.

CRediT authorship contribution statement

Guofeng Xu: Conceptualization, Methodology, Validation, Formal analysis, Investigation, Data curation, Writing – original draft. **Liang Luo:** Resources. **Jianwen Liang:** Formal analysis, Writing – review & editing, Investigation. **Shangqian Zhao:** Resources, Methodology.

Rong Yang: Resources, Investigation. **Changhong Wang:** Formal analysis, Writing – review & editing, Investigation. **Tianwei Yu:** Formal analysis. **Limin Wang:** Resources, Investigation. **Wei Xiao:** Resources, Investigation. **Jiantao Wang:** Conceptualization, Supervision, Funding acquisition. **Jinqiu Yu:** Resources, Supervision. **Xueliang Sun:** Supervision, Conceptualization.

Declaration of Competing Interest

The authors declare that they do not have any commercial or associative interest that represents a conflict of interest in connection with the work submitted.

Acknowledgements

Appendix A. Supporting information

Supplementary data associated with this article can be found in the online version at doi:10.1016/j.nanoen.2021.106674.

References

[1] J.B. Goodenough, Y. Kim, Challenges for rechargeable Li batteries, Chem. Mater. 22 (2010) 587–603.

[2] J. Janek, W.G. Zeier, A solid future for battery development, Nat. Energy 1 (2016) 16141.

[3] A. Manthiram, X. Yu, S. Wang, Lithium battery chemistries enabled by solid-state electrolytes, Nat. Rev. Mater. 2 (2017) 16103.

[4] T. Famprikis, P. Canepa, J.A. Dawson, M.S. Islam, C. Masquelier, Fundamentals of inorganic solid-state electrolytes for batteries, Nat. Mater. 18 (2019) 1278–1291.

[5] S. Kaboli, H. Demers, A. Paolella, A. Darwiche, M. Dontigny, D. Clement, A. Guerfi, M.L. Trudeau, J.B. Goodenough, K. Zaghib, Behavior of solid electrolyte in Li-polymer battery with NMC cathode via in-situ scanning electron microscopy, Nano Lett. 20 (2020) 1607–1613.

[6] S. Stramare, V. Thangadurai, W. Weppner, Lithium lanthanum titanates: a review, Chem. Mater. 15 (2003) 3974–3990.

[7] J. van den Broek, S. Afyon, J.L.M. Rupp, Interface-engineered all-solid-state Li-Ion batteries based on garnet-type fast Li+ conductors, Adv. Energy Mater. 6 (2016), 1600736.

[8] S. Kim, H. Oguchi, N. Toyama, T. Sato, S. Takagi, T. Otomo, D. Arunkumar, N. Kuwata, J. Kawamura, S.I. Orimo, A complex hydride lithium superionic conductor for high-energy-density all-solid-state lithium metal batteries, Nat. Commun. 10 (2019) 1081.

[9] L. Duchêne, A. Remhof, H. Hagemann, C. Battaglia, Status and prospects of hydroborate electrolytes for all-solid-state batteries, Energy Storage Mater. 25 (2020) 782–794.

[10] A. Sakuda, A. Hayashi, M. Tatsumisago, Interfacial observation between $LiCoO_2$ electrode and $Li_2S-P_2S_5$ Solid electrolytes of all-solid-state lithium secondary batteries using transmission electron microscopy, Chem. Mater. 22 (2009) 949–956.

[11] N. Kamaya, K. Homma, Y. Yamakawa, M. Hirayama, R. Kanno, M. Yonemura, T. Kamiyama, Y. Kato, S. Hama, K. Kawamoto, A. Mitsui, A lithium superionic conductor, Nat. Mater. 10 (2011) 682–686.

[12] Y. Zhu, Y. Mo, Materials design principles for air-stable lithium/sodium solid electrolytes, Angew. Chem. Int. Ed. 59 (2020) 17472–17476.

[13] Y. Li, X. Wang, H. Zhou, X. Xing, A. Banerjee, J. Holoubek, H. Liu, Y.S. Meng, P. Liu, Thin solid electrolyte layers enabled by nanoscopic polymer binding, ACS Energy Lett. 5 (2020) 955–961.

[14] Y. Kato, S. Hori, T. Saito, K. Suzuki, M. Hirayama, A. Mitsui, M. Yonemura, H. Iba, R. Kanno, High-power all-solid-state batteries using sulfide superionic conductors, Nat. Energy 1 (2016) 16030.

[15] T. Asano, A. Sakai, S. Ouchi, M. Sakaida, A. Miyazaki, S. Hasegawa, Solid halide electrolytes with high lithium-ion conductivity for application in 4 V class bulk-type all-solid-state batteries, Adv. Mater. 30 (2018), 1803075.

[16] X. Li, J. Liang, J. Luo, M.N. Banis, C. Wang, W. Li, S. Deng, C. Yu, F. Zhao, Y. Hu, T.-K. Sham, L. Zhang, S. Zhao, S. Lu, H. Huang, R. Li, K.R. Adaira, X. Sun, Air-stable Li_3InCl_6 electrolyte with high voltage compatibility for all-solid-state batteries, Energy Environ. Sci. 12 (2019) 2665–2671.

[17] X. Li, J. Liang, N. Chen, J. Luo, K.R. Adair, C. Wang, M.N. Banis, T.-K. Sham, L. Zhang, S. Zhao, S. Lu, H. Huang, R. Li, X. Sun, Water-mediated synthesis of a superionic halide solid electrolyte, Angew. Chem. Int. Ed. 58 (2019) 16427–16432.

[18] R. Schlem, S. Muy, N. Prinz, A. Banik, Y. Shao-Horn, M. Zobel, W.G. Zeier, Mechanochemical synthesis: a tool to tune cation site disorder and ionic transport properties of Li_3MCl_6 (M = Y, Er) superionic conductors, Adv. Energy Mater. 10 (2019), 1903719.

[19] J. Liang, X. Li, S. Wang, K.R. Adair, W. Li, Y. Zhao, C. Wang, Y. Hu, L. Zhang, S. Zhao, S. Lu, H. Huang, R. Li, Y. Mo, X. Sun, Site-occupation-tuned superionic Li_xScCl_{3+x} halide solid electrolytes for all-solid-state batteries, J. Am. Chem. Soc. 142 (2020) 7012–7023.

[20] J. Liang, E. van der Maas, J. Luo, X. Li, N. Chen, K. Adair, W. Li, Y. Hu, J. Li, L. Zhang, S. Zhao, S. Lu, H. Huang, S. Parnell, R. Smith, S. Ganapathy, M. Wagemaker, X. Sun, New series of ternary metal chloride superionic conductors for high performance all-solid-state lithium batteries, Nat. Commun. (2021), https://doi.org/10.21203/rs.3.rs-150360/v1.

[21] K.-H. Park, K. Kaup, A. Assoud, Q. Zhang, X. Wu, L.F. Nazar, High-voltage superionic halide solid electrolytes for all-solid-state Li-ion batteries, ACS Energy Lett. 5 (2020) 533–539.

[22] B. Helm, R. Schlem, B. Wankmiller, A. Banik, A. Gautam, J. Ruhl, C. Li, M. R. Hansen, W.G. Zeier, Exploring aliovalent substitutions in the lithium halide superionic conductor $Li_{3-x}In_{1-x}Zr_xCl_6$ (0≤x≤0.5), Chem. Mater. 33 (2021) 4773–4782.

[23] H. Kwak, D. Han, J. Lyoo, J. Park, S.H. Jung, Y. Han, G. Kwon, H. Kim, S.-T. Hong, K.-W. Nam, Y.S. Jung, New Cost-effective halide solid electrolytes for all-solid-state batteries: mechanochemically prepared Fe^{3+}-substituted Li_2ZrCl_6, Adv. Energy Mater. 11 (2021), 2003190.

[24] S.Y. Kim, K. Kaup, K.-H. Park, A. Assoud, L. Zhou, J. Liu, X. Wu, L.F. Nazar, Lithium ytterbium-based halide solid electrolytes for high voltage all-solid-state batteries, ACS Mater. Lett. 3 (2021) 930–938.

[25] J. Park, D. Han, H. Kwak, Y. Han, Y.J. Choi, K.-W. Nam, Y.S. Jung, Heat treatment protocol for modulating ionic conductivity via structural evolution of $Li_{3-x}Y_{1-x}M_xCl_6$ (M= Hf^{4+}, Zr^{4+}) new halide superionic conductors for all-solid-state batteries, Chem. Eng. J. 425 (2021), 130630.

[26] S. Muy, J. Voss, R. Schlem, R. Koerver, S.J. Sedlmaier, F. Maglia, P. Lamp, W. G. Zeier, Y. Shao-Horn, High-throughput screening of solid-state li-ion conductors using lattice-dynamics descriptors, iScience 16 (2019) 270–282.

[27] C. Yu, Y. Li, K.R. Adair, W. Li, K. Goubitz, Y. Zhao, M.J. Willans, M.A. Thijs, C. Wang, F. Zhao, Q. Sun, S. Deng, J. Liang, X. Li, R. Li, T.-K. Sham, H. Huang, S. Lu, S. Zhao, L. Zhang, Lv Eijck, Y. Huang, X. Sun, Tuning ionic conductivity and electrode compatibility of Li_3YBr_6 for high-performance all solid-state Li batteries, Nano Energy 77 (2020), 105097.

[28] Z. Liu, S. Ma, J. Liu, S. Xiong, Y. Ma, H. Chen, High ionic conductivity achieved in $Li_3Y(Br_3Cl_3)$ mixed halide solid electrolyte via promoted diffusion pathways and enhanced grain boundary, ACS Energy Lett. 6 (2020) 298–304.

[29] L. Zhou, C.Y. Kwok, A. Shyamsunder, Q. Zhang, X. Wu, L.F. Nazar, A new halospinel superionic conductor for high-voltage all solid state lithium batteries, Energy Environ. Sci. 13 (2020) 2056–2063.

[30] X. Li, J. Liang, K.R. Adair, J. Li, W. Li, F. Zhao, Y. Hu, T.-K. Sham, L. Zhang, S. Zhao, S. Lu, H. Huang, R. Li, N. Chen, X. Sun, Origin of superionic $Li_3Y_{1-x}In_xCl_6$ halide solid electrolytes with high humidity tolerance, Nano Lett. 20 (2020) 4384–4392.

[31] S.-K. Jung, H. Gwon, G. Yoon, L.J. Miara, V. Lacivita, J.-S. Kim, Pliable lithium superionic conductor for all-solid-state batteries, ACS Energy Lett. 6 (2021) 2006–2015.

[32] Y. Han, S.H. Jung, H. Kwak, S. Jun, H.H. Kwak, J.H. Lee, S.T. Hong, Y.S. Jung, Single-or poly-crystalline Ni-rich layered cathode, sulfide or halide solid electrolyte: which will be the winners for all-solid-state batteries? Adv. Energy Mater. 11 (2021), 2100126.

[33] C. Wang, J. Liang, M. Jiang, X. Li, S. Mukherjee, K. Adair, M. Zheng, Y. Zhao, F. Zhao, S. Zhang, R. Li, H. Huang, S. Zhao, L. Zhang, S. Lu, C.V. Singh, X. Sun, Interface-assisted in-situ growth of halide electrolytes eliminating interfacial challenges of all-inorganic solid-state batteries, Nano Energy 76 (2020), 105015.

[34] C. Zhao, J. Liang, X. Li, N. Holmes, C. Wang, J. Wang, F. Zhao, S. Li, Q. Sun, X. Yang, J. Liang, X. Lin, W. Li, R. Li, S. Zhao, H. Huang, L. Zhang, S. Lu, X. Sun, Halide-based solid-state electrolyte as an interfacial modifier for high performance solid-state $Li-O_2$ batteries, Nano Energy 75 (2020), 105036.

[35] L.M. Riegger, R. Schlem, J. Sann, W.G. Zeier, J. Janek, Lithium-metal anode instability of the superionic halide solid electrolytes and the implications for solid-state batteries, Angew. Chem. Int. Ed. 60 (2021) 6718–6723.

[36] B. Zahiri, A. Patra, C. Kiggins, A.X.B. Yong, E. Ertekin, J.B. Cook, P.V. Braun, Revealing the role of the cathode–electrolyte interface on solid-state batteries, Nat. Mater. 20 (2021) 1392–1400, https://doi.org/10.1038/s41563-021-01016-0.

[37] J. Hu, K. Chen, C. Li, Nanostructured Li-rich fluoride coated by ionic liquid as high ionconductivity solid electrolyte additive to suppress dendrite growth at Li metal anode, ACS Appl. Mater. Interfaces 10 (2018) 34322–34331.

[38] J. Hu, Z. Yao, K. Chen, C. Li, High-conductivity open framework fluorinated electrolyte bonded by solidified ionic liquid wires for solid-state Li metal batteries, Energy Storage Mater. 28 (2020) 37–46.

[39] W. Zhang, T. Leichtweiss, S.P. Culver, R. Koerver, D. Das, D.A. Weber, W.G. Zeier, J. Janek, The detrimental effects of carbon additives in $Li_{10}GeP_2S_{12}$-based solid-state batteries, ACS Appl. Mater. Interfaces 9 (2017) 35888–35896.

[40] S. Boulineau, M. Courty, J.-M. Tarascon, V. Viallet, Mechanochemical synthesis of Li-argyrodite Li_6PS_5X (X—Cl, Br, I) as sulfur-based solid electrolytes for all solid state batteries application, Solid State Ion. 221 (2012) 1–5.

[41] A.M. Nolan, Y. Zhu, X. He, Q. Bai, Y. Mo, Computation-accelerated design of materials and interfaces for all-solid-state lithium-ion batteries, Joule 2 (2018) 2016–2046.

[42] W.D. Richards, L.J. Miara, Y. Wang, J.C. Kim, G. Ceder, Interface stability in solid-state batteries, Chem. Mater. 28 (2015) 266–273.

[43] S. Wang, Q. Bai, A.M. Nolan, Y. Liu, S. Gong, Q. Sun, Y. Mo, Lithium chlorides and bromides as promising solid-state chemistries for fast ion conductors with good electrochemical stability, Angew. Chem. Int. Ed. 58 (2019) 8123–8127.

[44] S.P. Ong, O. Andreussi, Y. Wu, N. Marzari, G. Ceder, Electrochemical windows of room-temperature ionic liquids from molecular dynamics and density functional theory calculations, Chem. Mater. 23 (2011) 2979–2986.

[45] D. Park, H. Park, Y. Lee, S.-O. Kim, H. Jung, K.Y. Chung, J.H. Shim, S. Yu, Theoretical design of lithium chloride superionic conductors for all-solid-state high voltage lithium-ion batteries, ACS Appl. Mater. Interfaces 12 (2020) 34806–34814.

[46] J. Heyd, G.E. Scuseria, Efficient hybrid density functional calculations in solids: assessment of the Heyd-Scuseria-Ernzerhof screened Coulomb hybrid functional, J. Chem. Phys. 121 (2004) 1187–1192.

[47] A. Mielke, Ferromagnetism in the Hubbard model and Hund's rule, Phys. Lett. A 174 (1993) 443–448.

[48] K. Held, D. Vollhardt, Microscopic conditions favoring itinerant ferromagnetism: Hund's rule coupling and orbital degeneracy, Eur. Phys. J. B 5 (1998) 473–478.

[49] X. Li, J. Liang, X. Yang, K.R. Adair, C. Wang, F. Zhao, X. Sun, Progress and perspectives on halide lithium conductors for all-solid-state lithium batteries, Energy Environ. Sci. 13 (2020) 1429–1461.

[50] N. Tanibata, S. Takimoto, K. Nakano, H. Takeda, M. Nakayama, H. Sumi, Metastable chloride solid electrolyte with high formability for rechargeable all-solid-state lithium metal batteries, ACS Mater. Lett. 2 (2020) 880–886.

[51] B. Ravel, M. Newville, Athena, Artemis, Hephaestus: data analysis for X-ray absorption spectroscopy using IFEFFIT, J. Synchrotron Radiat. 12 (2005) 537–541.

[52] Y. Okamoto, H. Motohashi, XAFS study of molten $ZrCl_4$ in LiCl-KCl eutectic, Z. Naturforsch A 57 (2002) 277–280.

Dr. Guofeng Xu received his Ph.D. degree in metallurgical engineering from University of Science and Technology Beijing in 2017. Then he joined the China Automotive Battery Research Institute, where he continued his research on advanced cathode oxides, solid-state electrolytes as well as all-solid-state Li-ion batteries.

Dr. Changhong Wang is currently a research scientist in GLABAT Solid-State Inc. Canada. He obtained his M.S. degree in Materials Engineering in 2014 from University of Science and Technology of China (USTC) and received his Ph.D. degree in Mechanical and Materials Engineering from the University of Western Ontario (UWO), Canada. He also served as a research assistant in Singapore University of Technology and Design (SUTD) from 2014 to 2016. Currently, his research interests include solid-state sulfide electrolytes, all-solid-state batteries, and bio-inspired artificial synapses.

Liang Luo is a research engineer in Rare Earth Functional Materials (Xiong'an) Innovation Center Co., Ltd. and National Engineering Research Center for Rare Earth Materials, GRINM Group Co., Ltd. He received his M.S. degree in 2018 from Xinjiang Technical Institute of Physics and Chemistry, Chinese Academy of Sciences. His current research focuses on the application of rare earth halides in solid-state electrolytes and scintillation crystals.

Yu Tianwei is currently is currently a PhD candidate in Prof. Jiantao Wang's Group at the Department of Innovation in China Automotive Battery Research Institute Co., Ltd and General Research Institute for Nonferous Metals. He received his Bachelor's degree in Materials Science and Engineering from Beijing University of Technology in 2018. Currently, he is working on the synthesis and characterization of halide solid-state electrolytes and the development of high performance solid-state lithium metal batteries.

Dr. Jianwen Liang is a Mitacs Postdoc Fellow in Prof. Xueliang (Andy) Sun's Group at the University of Western Ontario (Western Univeriity), Canada. He received his B.S. degree in Chemical Engineering and Technology from Wuyi University in 2010 and PhD degree in inorganic chemistry from the University of Science and Technology of China in 2015. He joined Prof. Sun's group in 2017 and his current research interests include sulfide and halide solid electrolytes as well as all-solid-state Li/Li-ion batteries.

Limin Wang is currently a Ph.D. candidate in Beijing General Research Institute for Nonferrous Metals. She received her bachelor's degree from YanShan university in 2018. Her current research interests focus on first principles calculation and the solid-state electrolyte.

Dr. Shangqian Zhao received his B.S.degree in Physics from Jilin University in 2009 and his Ph.D. degree in Condensed Matter Physics from Institute of Physics, Chinese Academy of Sciences in 2014. He is currently a senior scientist of China Automotive Battery Research Institute Co., Ltd., Beijing, China. His research interests focus on mass production of solid electrolytes and development of high-capacity solid-state Li/Li-ion batteries.

Dr. Wei Xiao is a senior engineer in GRIMAT Engineering Institute Co., Ltd. He received his B.S. degree in Material Physics in 2007 and Ph.D. degree in Material Physics & Chemistry in 2013 from University of Science and Technology Beijing. He also served as a research scholar in California State University, Northridge from 2011 to 2013. His research mainly focus on material genomics computing technology and theoretical design of nonferrous metals.

Prof. Rong Yang received his Ph.D. degree in inorganic chemistry from Peking University in 2011. He is currently professor in China Automotive Battery Research Institute. His research interests are focused on cathode materials for lithium-ion batteries, solid-state lithium ion conductors, and solid-state lithium-ion batteries.

Prof. Jiantao Wang is the general manager of Department of Innovation in China Automotive Battery Research Institute Co., Ltd, recipient of 2015 Beijing Nova program, professor in General Research Institute for Nonferous Metals. He obtained his B.S. in Analytical Chemistry from University of Science and Technology Beijing in 2006, and received his Ph.D. in Organic Chemistry in Technical Institute of Physics and Chemistry, Chinese Academy of Sciences, in 2011. His research interests include advanced electrode materials, high-energy Li-ion batteries and solid-state batteries.

Dr. Jinqiu Yu is a senior engineer in Rare Earth Functional Materials (Xiong'an) Innovation Center Co., Ltd. and National Engineering Research Center for Rare Earth Materials, GRINM Group Co., Ltd. He received his B.S. degree in chemistry from Wuhan University in 2006, and received his Ph.D. in physical chemistry from Technical Institute of Physics and Chemistry, Chinese Academy of Sciences, in 2011. His current research interests focus on the preparation technology of anhydrous rare earth halides and their applications in fields of scintillation crystals and solid-state electrolytes.

Prof. Xueliang Sun is a Canada Research Chair in Development of Nanomaterials for Clean Energy, Fellow of the Royal Society of Canada and Canadian Academy of Engineering and Full Professor at the University of Western Ontario, Canada. Dr. Sun received his Ph.D. in materials chemistry in 1999 from the University of Manchester, UK, which he followed up by working as a postdoctoral fellow at the University of British Columbia, Canada and as a Research Associate at L′Institut National de la Recherche Scientifique (INRS), Canada. His research interests are focused on advanced materials for electrochemical energy storage and conversion.